Title:

Genome editing in the unicellular holozoan *Capsaspora owczarzaki* suggests a premetazoan function for the Hippo pathway in multicellular morphogenesis

Authors:

Jonathan E Phillips[1], Maribel Santos[1], Mohammed Kanchwala[2], Chao Xing[2], Duojia Pan[1*]

Affiliations:

[1]Department of Physiology, Howard Hughes Medical Institute, University of Texas Southwestern Medical Center, Dallas, Texas 75390, USA

[2]Eugene McDermott Center for Human Growth & Development, Departments of Bioinformatics and Clinical Sciences, University of Texas Southwestern Medical Center, Dallas, Texas 75390, USA

* correspondence: duojia.pan@utsouthwestern.edu

ABSTRACT

Animal development is mediated by a surprisingly small set of canonical signaling pathways such as Wnt, Hedgehog, TGF-beta, Notch and Hippo pathways. Although once thought to be present only in animals, recent genome sequencing has revealed components of these pathways in the closest unicellular relatives of animals. These findings raise questions about the ancestral functions of these developmental pathways and their potential role in the emergence of animal multicellularity. Here, we provide the first functional characterization of any of these developmental pathways in unicellular organisms by developing techniques for genetic manipulation in *Capsaspora owczarzaki*, a close unicellular relative of animals that displays aggregative multicellularity. We then use these tools to characterize the *Capsaspora* ortholog of the Hippo signaling nuclear effector YAP/TAZ/Yorkie (coYki), a key regulator of tissue size in animals. In contrast to what might be expected based on studies in animals, we show that coYki is dispensable for cell proliferation but regulates cytoskeletal dynamics and the three-dimensional (3D) shape of multicellular structures. We further demonstrate that the cytoskeletal abnormalities of individual coYki mutant cells underlie the abnormal 3D shape of coYki mutant aggregates. Taken together, these findings implicate an ancestral role for the Hippo pathway in cytoskeletal dynamics and multicellular morphogenesis predating the origin of animal multicellularity, which was co-opted during evolution to regulate cell proliferation.

INTRODUCTION

The vast morphological diversity observed in animals is generated by developmental programs mediated by a surprisingly small set of conserved signaling pathways (Pires-daSilva and Sommer, 2003). An exciting and unexpected finding from comparative genomic analysis indicates that many components of these pathways are present in the closest unicellular relatives of animals (King et al., 2003; Ros-Rocher et al., 2021). This raises the question of whether these pathways show similar functions in animals and their unicellular relatives, and, if not, what the ancestral

42 functions of these pathways were, and how they evolved to function in multicellular processes in
43 animals. Answering this question could illuminate the roots of animal multicellularity and provide
44 novel perspective on how to manipulate the activity of these biomedically important pathways.
45
46 One such signaling pathway is the Hippo pathway, which coordinates cell proliferation,
47 differentiation, and survival in animals. Initially defined as a tumor suppressor pathway that
48 restricts tissue growth in *Drosophila* development, Hippo signaling plays a conserved role in organ
49 size control and regeneration in mammals (Davis and Tapon, 2019; Harvey and Hariharan, 2012;
50 Moya and Halder, 2018; Yu et al., 2015; Zheng and Pan, 2019). This pathway comprises a core
51 kinase cascade involving sequential activation of two kinases, Hpo/MST and Wts/LATS, which
52 culminates in the phosphorylation and inactivation of the potent growth-stimulatory transcriptional
53 coactivator YAP/TAZ/Yorkie. This core kinase cascade is in turn regulated by diverse upstream
54 inputs, most notably mechanical force, the state of the actin cytoskeleton, and cell-cell or cell-
55 substrate adhesion as part of a mechanotransduction pathway that relays mechanical and
56 architectural cues to gene expression. Echoing its pervasive function in metazoan growth control,
57 the Hippo pathway is required for contact-inhibition of proliferation in cultured mammalian cells,
58 and defective Hippo signaling leading to YAP/TAZ oncogene activation is a major driver of human
59 cancers (Davis and Tapon, 2019; Harvey and Hariharan, 2012; Moya and Halder, 2018; Yu et al.,
60 2015; Zheng and Pan, 2019).
61
62 The Hippo pathway was at one point thought to be specific to animals. However, genome
63 sequencing efforts have revealed that a core Hippo pathway and many upstream regulators are
64 encoded in the genomes of the closest unicellular relatives of animals such as choanoflagellates
65 and filasterians (Figure 1A) (Sebe-Pedros et al., 2012). The choanoflagellates are flagellated filter
66 feeders that can form multicellular rosette structures by incomplete cytokinesis (Fairclough et al.,
67 2010), whereas filasterians are amoeboid organisms characterized by actin-rich filopodial

68 projections (Figure 1, B and C) and represent the most basal known unicellular organism
69 encoding all core components of the Hippo pathway, including upstream kinases and downstream
70 transcriptional machinery (Sebe-Pedros et al., 2012). *Capsaspora owczarzaki* is a filasterean
71 originally isolated as a putative endosymbiont in the freshwater snail *B. glabrata* that can attack
72 and kill the parasitic schistosome *S. mansoni* (Stibbs et al., 1979). *Capsaspora* can be cultured
73 easily in axenic growth medium containing protein source and serum in adherent or shaking
74 culture and can be transiently transfected, allowing for the examination of protein localization
75 using fluorescent fusion proteins (Parra-Acero et al., 2018). Although *Capsaspora* tends to grow
76 as a unicellular organism in laboratory culture conditions, under certain conditions *Capsaspora*
77 cells can adhere to each other to form multicellular aggregates (Figure 1, D to F and Figure S1,
78 (Sebe-Pedros et al., 2013)), suggesting that multicellular behaviors may have been selected for
79 in the lineage leading to *Capsaspora*. Previously, we have shown that overexpression of
80 *Capsaspora* Hippo pathway components such as coYki and coHpo in *Drosophila* elicits similar
81 phenotypes as their *Drosophila* orthologs (Sebe-Pedros et al., 2012), suggesting that a functional
82 Hippo signaling pathway may have evolved well before the emergence of Metazoa. The
83 *Capsaspora* genome also encodes homologues of other key regulators of animal development
84 such as components of the integrin adhesome (Sebe-Pedros et al., 2010), cadherins (Nichols et
85 al., 2012), tyrosine kinases such as Src and Abl (Suga et al., 2012), NF-kB (Williams and Gilmore,
86 2020) and p53 (Sebe-Pedros et al., 2017). Thus, *Capsaspora* offers a unique opportunity to
87 elucidate the ancestral function of these important developmental regulators in a close unicellular
88 relative of animals.
89
90 **RESULTS**
91
92 **Development of genome editing tools in *Capsaspora owczarzaki* enables genetic**
93 **disruption of a YAP/TAZ/Yorkie ortholog**

94 In an effort to make *Capsaspora* a tractable system for evolutionary cell biology studies, we
95 developed genetic tools for overexpression and loss-of-function analysis. We first established a
96 method for engineering stable *Capsaspora* cell lines by transfecting a vector encoding the
97 fluorescent protein mScarlet and resistance to the antibiotic Geneticin (GenR). After transfection,
98 antibiotic selection, and generation of clonal lines by serial dilution, we were able to generate
99 uniformly mScarlet-positive clonal populations of cells (Figure S2A**)**. Transfection of *Capsaspora*
100 with genes encoding resistance to nourseothricin (NatR) or hygromycin (HygR) followed by
101 selection with the respective antibiotic could also generate drug-resistant transformants (Figure
102 S2B). These results demonstrate that stable *Capsaspora* cell lines expressing multiple
103 transgenes can be generated.
104
105 We next sought to develop tools for loss-of-function analysis in *Capsaspora*. After unsuccessful
106 attempts at CRISPR-Cas9-mediated genome editing, which may be due to the lack of
107 nonhomologous end joining machinery components in *Capsaspora*, we used PCR-generated
108 targeting constructs to achieve gene disruption by homologous recombination, replacing each
109 allele of a diploid *Capsaspora* gene with a distinct selectable antibiotic marker (Figure 1G). This
110 strategy allowed us to generate a cell line in which both *coYki* alleles were disrupted (Figure S2
111 C-E), with no detectable expression of the deleted region of *coYki* **(**Figure 1, H to J**)**. These results
112 demonstrate the generation of a homozygous *coYki* disruption mutant (subsequently *coYki -/-*)
113 and establish a method for the generation of mutants by gene targeting in *Capsaspora.*
114
115 **coYki is dispensable for cell proliferation but regulates the 3D shape of multicellular**
116 **structures**
117 To determine the effect of coYki on cell proliferation, we examined the proliferation of *Capsaspora*
118 cells in adherent or shaking culture. In contrast to what may be expected based on previous

119 studies in animal cells, we observed no significant difference in cell proliferation between WT and
120 *coYki -/-* cells in either condition (Figure S3). We next sought to examine cell proliferation within
121 *Capsaspora* aggregates. Previously, aggregates have been generated by gentle shaking of cell
122 cultures (Sebe-Pedros et al., 2013). To make aggregates more amenable to extended imaging *in*
123 *situ*, we developed a condition that induced robust aggregate formation by plating *Capsaspora*
124 cells in low-adherence wells (Figure 1, D to F). Under this condition, most cells coalesced into
125 aggregates over 2-3 days, leaving few isolated cells in the culture. Treatment with the calcium
126 chelator EGTA resulted in rapid dissociation of the aggregates (Figure S1), suggesting that
127 calcium-dependent cell adhesion mediates aggregate integrity. We used EdU incorporation to
128 label proliferating cells in aggregates, and observed no significant difference in the percent of
129 EdU-positive cells between WT and *coYki -/-* genotypes (Figure 2, A and B). Unlike clones of
130 cultured mammalian cells that often display increased cell proliferation at the clonal boundary
131 (Fisher and Yeh, 1967), distribution of EdU+ cells was homogeneous within *Capsaspora*
132 aggregates (Figure 2A), suggesting that a mechanism akin to contact-mediated inhibition of
133 proliferation is absent in *Capsaspora*. Together, these results suggest that the rate of proliferation
134 of *Capsaspora* is independent of coYki or contact inhibition.
135
136 While examining *Capsaspora* aggregates, we observed a profound phenotype in the shape of the
137 *coYki -/-* aggregates. After aggregate induction by plating cells in low-adherence conditions, WT
138 cell aggregates showed a round morphology (Figure 2C). In contrast, *coYki -/-* aggregates were
139 asymmetric and less circular than WT aggregates (Figure 2D). Computational analysis of
140 aggregate morphology and size revealed that WT and *coYki -/-* aggregate size was not
141 significantly different (Figure 2E), whereas *coYki -/-* aggregates were significantly less circular
142 than WT aggregates (Figure 2F). Optical sectioning of aggregates expressing mScarlet showed
143 that WT aggregates were thicker perpendicular to the culture surface and more spherical than

144 *coYki -/-* aggregates (Figure 2G). Time-lapse microscopy of aggregation over a period of six days
145 showed that, whereas WT cells accreted into round aggregates that fused with other aggregates
146 when in close proximity but never underwent fission, *coYki -/-* aggregates were dynamically
147 asymmetrical, less circular than WT, and sometimes underwent fission (Video S1). Taken
148 together, these findings uncover a critical role for coYki in 3-dimensional (3D) shape of
149 aggregates, but not cell proliferation, in *Capsaspora*.
150
151 **Loss of coYki affects cell-substrate adhesion but not cell-cell adhesion**
152 Cell-cell adhesion and cell-substrate adhesion affect 3D shape of tumor cell aggregates (Blandin
153 et al., 2016; Saias et al., 2015). We therefore tested whether cell-cell adhesion and cell-substrate
154 adhesion differ in WT *and coYki -/- cells.* A prediction of differential cell-cell adhesion is that
155 mosaic aggregates of WT and *coYki -/-* cells may show cell sorting within aggregates (Foty and
156 Steinberg, 2005). To test this prediction, we induced aggregate formation after mixing mCherry-
157 labeled WT or *coYki* -/- cells with unlabeled WT cells at 1:9 ratio. The distribution of mCherry-
158 labeled WT or *coYki* -/- cells within such mixed aggregates was similar and no cell sorting was
159 evident (Figure 3, A to D)**,** indicating that individual *coYki -/-* cells are competent to adhere to and
160 integrate within aggregates and suggesting that the aberrant morphology of *coYki -/-* aggregates
161 is an emergent property of a large number of *coYki -/-* cells.
162
163 To further test whether cell-cell adhesion differs in WT and *coYki -/-* cells, we vigorously vortexed
164 *Capsaspora* cultures to separate individual cells, allowed cell clusters to form by cell-cell adhesion
165 under gentle rotation, and then counted the number of cells in each cluster. The number of cells
166 per cluster was similar for WT and *coYki -/-* cells (Figure 3E), suggesting that the occurrence of
167 cell-cell adhesion is similar in these genotypes. We next tested whether cell-substrate adhesion
168 differed in WT and *coYki -/-* cells by agitating cultures of adherent cells and counting the number
169 of cells that disassociate from the culture surface. After agitation, significantly more *coYki* -/- cells

170 remained attached to the culture surface compared to WT cells (Figure 3F), indicating that coYki
171 negatively regulates cell-substrate adhesion. Together, our data suggest that coYki affects the
172 morphology of cell aggregates by affecting cell-substrate adhesion but not cell-cell adhesion.
173
174 ***coYki -/-* cells show aberrant cytoskeletal dynamics and bleb-like protrusions**
175 To characterize properties of *coYki -/-* cells that may contribute to abnormal aggregate
176 morphology, we used time-lapse microscopy to examine the dynamic morphology of individual
177 WT and *coYki -/-* cells in adherent culture. Interestingly, the cortices of *coYki -/-* cells were much
178 more dynamic than those of WT cells. Whereas *coYki -/-* cells display extensive membrane
179 protrusions and retractions, such dynamic membrane structures were rarely observed in WT cells
180 (Video S2). To characterize the differences in cell membrane dynamics, we quantified the
181 occurrence of cell protrusions in WT cells, *coYki -/-* cells, and *coYki -/-* cells expressing a *coYki*
182 rescue transgene. WT cells rarely showed protrusions. In contrast, *coYki -/-* cells showed an
183 average of 3.1 protrusions per minute (Figure 4A), a phenotype that was rescued in *coYki -/-* cells
184 expressing a *coYki* transgene (Figure 4A, Video S3). These results suggest that coYki affects the
185 cortical dynamics of *Capsaspora* cells.
186
187 In principle, the extensive membrane protrusions made by *coYki -/-* cells may represent F-actin-
188 rich pseudopodia, which drive amoeboid motility, or, alternatively, F-actin-poor blebs, which are
189 actin-depleted extensions of plasma membrane generated by disassociation of the membrane
190 from the cell cortex or cortical rupture (Charras and Paluch, 2008). To distinguish between these
191 possibilities, we stably expressed a fusion protein of the F-actin-binding Lifeact peptide (Riedl et
192 al., 2008) with mScarlet in WT and *coYki -/-* cells and examined F-actin dynamics by time-lapse
193 microscopy. At the basal side of WT cells, Lifeact-mScarlet was often enriched at the cell edge
194 corresponding to the direction of cell movement, suggesting that *Capsaspora* undergoes F-actin-
195 mediated amoeboid locomotion (Video S4)**.** As cells move, some Lifeact-mScarlet signal appears

196 as stationary foci on the basal surface, suggesting the existence of actin-rich structures that
197 mediate cell-substrate interaction in *Capsaspora* (Figure 4B, Video S4). Optical sections at mid-
198 height of WT cells showed that F-actin was enriched at a circular cell cortex, where transient
199 bursts of small F-actin puncta were often observed (Figure 4B, Video S5). In contrast, cortical
200 shape was less circular in *coYki -/-* cells, and F-actin concentration along the cortex was less
201 uniform (Figure 4B). During the formation of the membrane protrusions produced by *coYki -/-*
202 cells, F-actin was initially depleted as compared to the rest of the cell (Figure 4C, Video S6). After
203 the membrane protrusions had fully extended, F-actin accumulated first at the distal end and then
204 along the entire cortex of the protrusion, followed by the regression of the protrusion. A similar
205 sequence of cytoskeletal events occurs in blebbing mammalian cells (Charras et al., 2006). These
206 results suggest that the protrusions observed in *coYki -/-* cells are actin-depleted blebs, and that
207 after bleb formation, F-actin re-accumulates within the bleb leading to cortical reformation and
208 bleb regression.
209
210 To determine whether the abnormal cortical cytoskeleton is specific to *coYki -/-* cells in adherent
211 culture, we examined *coYki -/-* cells within aggregates by time-lapse microscopy. Lifeact-
212 mScarlet-expressing cells were mixed with cells stably expressing the green fluorescent protein
213 Venus so that Lifeact-mScarlet-expressing cells were well-spaced and able to be imaged
214 individually. As in adherent cells, *coYki -/-* cells within aggregates showed dynamic formation of
215 actin-depleted blebs (Video S7). Thus, *coYki -/-* cells show aberrant cortical cytoskeleton and
216 excessive membrane blebbing in both isolated adherent cells and within aggregates.
217
218 **Treatment of *coYki -/-* cells with blebbistatin rescues both membrane blebbing and**
219 **aberrant shape of multicellular aggregates**
220 Loss of coYki causes both bleb-like protrusions and abnormal aggregate morphology, suggesting
221 that the cellular phenotypes observed in *coYki -/-* cells (membrane blebbing and related cortical

222 cytoskeletal defects) may underlie the aberrant aggregate morphology. We tested this hypothesis
223 by treating *coYki -/-* cells with Blebbistatin, a myosin II inhibitor named after its bleb-inhibiting
224 activity in mammalian cells (Straight et al., 2003). Strikingly, not only did low concentrations of
225 Blebbistatin suppress the formation of blebs in *coYki -/-* cells (Figure 4D, Video S8), Blebbistatin
226 also rescued the abnormal morphology of *coYki -/-* aggregates (Figure 4E). Whereas *coYki -/-*
227 cell aggregates were asymmetric and showed low circularity (Figure 4E'''), *coYki -/-* aggregates
228 treated with blebbistatin were circular and resembled WT aggregates (Figure 4E'''' and 4F). These
229 results suggest a causal link between the membrane/cytoskeletal defects observed in individual
230 *coYki -/-* cells and the abnormal morphology of *coYki -/-* aggregates.
231

232 **Gene expression changes in *coYki -/-* cells support a role for coYki in cytoskeletal**
233 **functions**

234 To characterize the transcriptional targets of coYki that may underlie the
235 morphological/cytoskeletal defects of *coYki -/-* cells, we performed RNAseq on WT and *coYki -/-*
236 cells in adherent culture. This analysis revealed 1205 differentially expressed genes, including
237 397 downregulated and 808 upregulated genes in the *coYki* mutant. Functional enrichment
238 analysis of these two gene sets revealed distinct enrichment of functional categories (Figure 5, A
239 and B). Genes predicted to encode actin-binding proteins were enriched in the set of genes
240 upregulated in the *coYki -/-* mutant, suggesting that these genes may play a role in the aberrant
241 cytoskeletal dynamics observed in *coYki -/- cells.* To further inquire into the potential function of
242 coYki-regulated genes, we searched the 1205 differentially expressed genes against a previously
243 reported *Capsaspora* phylome (Sebe-Pedros et al., 2016) to identify 638 *Capsaspora* genes with
244 predicted human or mouse orthologs. Ingenuity Pathway Analysis of this mammalian ortholog set
245 showed that the two most significantly enriched functional categories corresponded to cell
246 movement and cell migration (Figure 5C). Notably, regulation of cell migration was reported as
247 the most enriched functional category among YAP target genes in glioblastoma cells (Stein et al.,

248 2015), and cell motility was an enriched category in an integrative analysis of gene regulatory
249 networks downstream of YAP/TAZ utilizing transcriptomic and cistromic data from multiple human
250 tissues (Paczkowska et al., 2020). However, in contrast to functional enrichment studies in
251 metazoan systems examining genes regulated by YAP/TAZ/Yorkie (Ikmi et al., 2014; Stein et al.,
252 2015; Zanconato et al., 2015), no enrichment was detected in functional categories of cell
253 proliferation or the cell cycle (Figure 5C). This finding is consistent with the lack of a proliferative
254 phenotype in *coYki -/-* cells.
255
256 **DISCUSSION**
257
258 Given that all current biological phenomena are the product of a long and complex evolutionary
259 process, understanding the evolutionary history of biological systems, such as signaling
260 pathways, can give important insight into their current properties and functions. The presence of
261 complete core Hippo pathway components in the close unicellular relatives of animals (Sebe-
262 Pedros et al., 2012) provides the opportunity to elucidate the premetazoan function and
263 evolutionary history of this pathway. By developing tools for genome editing in *Capsaspora*, we
264 demonstrate that coYki regulates cytoskeletal dynamics at the cell cortex but is dispensable for
265 the proliferation of *Capsaspora* cells. Such coYki-dependent cortical cytoskeletal function, in turn,
266 regulates the 3D shape of *Capsaspora* aggregates in a manner that may involve tuning the
267 strength of cell-substrate adhesion. Investigating the Hippo pathway in other unicellular relatives
268 of animals such as choanoflagellates and ichthyosporeans, which are now amenable to
269 transgenic studies (Booth and King, 2020; Booth et al., 2018; Suga and Ruiz-Trillo, 2013), will
270 further clarify the ancestral function of this pathway predating the emergence of animal
271 multicellularity.
272

273 Our findings implicate cytoskeletal regulation as an ancestral function of the Hippo pathway
274 predating the origin of Metazoa, and that this pathway was later co-opted to control cell
275 proliferation after the unicellular-to-multicellular transition in the lineage leading to animals. This
276 co-option likely occurred early in the animal lineage, as in early-diverging ctenophores and
277 cnidarians Hippo pathway activity is enriched in proliferating tissues (Coste et al., 2016). Given
278 that the cortical cytoskeleton is both an important upstream regulator and a downstream effector
279 of Hippo signaling in animal cells (Deng et al., 2020; Fernandez et al., 2011; Gaspar and Tapon,
280 2014; Sun and Irvine, 2016), the co-option of the Hippo pathway for cell proliferation control in
281 early metazoans may have provided a convenient mechanism that couples cell proliferation with
282 cytoskeletal and mechanical properties of cells.
283
284 Our study suggests that the abnormal 3D shape of *coYki -/-* aggregates is due to increased cell-
285 substrate adhesion without affecting cell-cell adhesion. *Capsaspora* encodes an integrin
286 adhesome (Sebe-Pedros et al., 2010), and *Capsaspora* cell-substrate adhesion is mediated at
287 least in part by integrins (Parra-Acero et al., 2020). Indeed, our RNA-seq data shows that two
288 integrin-β genes (CAOG_05058 and CAOG_01283) are upregulated in *coYki -/-* cells, suggesting
289 a potential contribution by integrins in this phenotype. Given that the strength of integrin-mediated
290 focal adhesions can be regulated by cytoskeletal contractility (Dumbauld et al., 2010), the
291 aberrant cytoskeletal properties of *coYki -/-* cells may also contribute to their abnormal cell-
292 substrate adhesion. This possibility is consistent with our data showing that blebbistatin, which
293 inhibits myosin and thus perturbs cytoskeletal contractility, can rescue the aberrant morphology
294 of *coYki -/-* aggregates.
295
296 A dedicated role for coYki in regulating the 3D shape but not the size of *Capsaspora* aggregates
297 may reflect the different selection pressures on animals versus their close unicellular relatives. It
298 has been suggested that the emergence of multicellularity is driven by phagotrophic predators of

299 unicellular organisms, as multicellular aggregates are less likely to be consumed by phagotrophic
300 predators and thus are selectively favored (Stanley, 1973). A round aggregate shape ensures
301 maximum contact between cells within the group, reducing the chance of a cell disassociating
302 and thus being vulnerable to predation. Interestingly, a YAP loss-of-function mutation in medaka
303 fish causes a tissue flattening phenotype (Porazinski et al., 2015) similar to that observed in *coYki*
304 *-/- Capsaspora* aggregates (Figure 5D). This suggests that the regulation of 3D tissue architecture
305 is an ancient and conserved function of YAP/TAZ/Yorkie predating the origin of animal
306 multicellularity. We suggest that YAP/TAZ/Yorkie may have first been selected during evolution
307 to regulate the 3D shape of multicellular aggregates in unicellular ancestors of animals, and
308 evolved later to also control organ size in order to maintain appropriate scaling between the size
309 of an organ and the size of the body as a whole.
310
311 Besides implicating an ancestral function of the Hippo pathway in pre-metazoan multicellular
312 morphogenesis, the genetic tools we have developed for modifying the *Capsaspora* genome
313 provide a valuable opportunity to interrogate the premetazoan functions of other developmental
314 regulators that are present in the genomes of close unicellular relatives of animals. Future
315 functional studies in *Capsaspora* and other close unicellular relatives of animals should clarify the
316 evolutionary history of these important signaling pathways and further elucidate the nature of the
317 unicellular ancestor of animals and the emergence of animal multicellularity.
318
319

320 **METHODS**

321

322 Cell culture

323 *Capsaspora* cells were maintained in ATCC Medium 1034 (modified PYNFH medium)
324 supplemented with 25 µg/mL Ampicillin (referred to below as "growth medium") in a 23°C
325 incubator. Cells were kept in either 25 cm^2 cell culture flasks in 8 mL medium or in 75 cm^2 cell
326 culture flasks in 15 ml medium. To induce cell aggregation, cells were resuspended to 7.5 x 10^5
327 cells/ml in growth medium, and 1 ml of this cell suspension was added per well to a 24-well ultra-
328 low attachment plate (Sigma CLS3473). To test the effect of blebbistatin on aggregate
329 morphology, a 20 mM stock solution of blebbistatin (Sigma B0560) in DMSO was made, and cells
330 were resuspended to 7.5 x 10^5 cells/ml in growth medium with 1 µm blebbistatin or DMSO only
331 as a vehicle control. Aggregates were then generated as described above and imaged with a
332 Nikon Eclipse Ti inverted microscope with NIS-Elements acquisition software.

333

334 To characterize cell proliferation during growth on a solid substrate, *Capsaspora* cells were diluted
335 to 1 x 10^5 cells/ml in growth medium, and 800 µl of this dilution was pipetted into multiple wells in
336 a 24-well polystyrene cell culture plate. To prevent edge effects, wells at the edge of the plate
337 were not used and were instead filled with 800 µl of water. The plates were then kept in in a 23°C
338 incubator. Each day, 1.5 µl of a 500 mM EDTA solution was added to a well, and cells in the well
339 were resuspended by pipetting up and down for one minute. Resuspended cells were then
340 transferred to a 1.5 mL tube, vortexed, and then the cell density was determined by
341 hemocytometer. To characterize cell proliferation in shaking culture, cells were diluted to 1 x 10^5
342 cells/ml in growth medium, and 20 ml of this dilution was added to a 125 ml Erlenmeyer culture
343 flask. Cultures were then incubated in an orbital shaker at 150 rpm and 23°C. Cell density was
344 determined daily by transferring 200 µl of culture to a 1.5 ml tube, adding 1.5 µl of 500 mM EDTA
345 solution to disassociate any aggregated cells, vortexing, and counting by hemocytometer.

346

347 Fixation and staining of aggregates

348 To fix and stain aggregates, aggregates were generated as described above, and then
349 aggregates were collected from a 24-well plate by gentle pipetting. 500 µl of aggregate
350 suspension was added dropwise to 9 ml of PM PFA (100 mM PIPES ph 6.9, 0.1 mM $MgSO_4$, 4%
351 PFA filtered through a 0.45 µm syringe filter) in a 15 mL polystyrene tube, and tubes were left
352 undisturbed for 1 hour to allow fixation. Aggregates were then centrifuged at 1000 x g for 3
353 minutes and resuspended in 500 µl of PEM buffer (100 mM PIPES pH 6.9, 1 mM EGTA, 0.1 mM
354 $MgSO_4$). After transferring aggregates to a microcentrifuge tube, aggregates were centrifuged for
355 2000 x g for 2 minutes, the supernatant was removed, and aggregates were resuspended in 300
356 µl of PEM.

357

358 As we found that aggregates were fragile during continued centrifugation-resuspension cycles,
359 we developed a protocol where solution changes could be done without centrifugation using 24-
360 well plate inserts with an 8 micron pore membrane at the insert base (Corning 3422). Before use
361 with aggregates, 100 µl PEM buffer was added to a well in a 24-well plate, 300 µl of PEM was
362 added to a membrane insert, and the insert was placed in the well and allowed to drain (contact
363 between the membrane and the solution within the well is critical for draining). Aggregates in 300
364 µl of PEM were added to the insert, and the insert was moved to a new well with 100 µl of PEM
365 and allowed to drain. As a wash step, the membrane insert was then moved to a well containing
366 1200 µl of PEM, allowing the membrane insert to fill with PEM buffer, and after a 5 minute
367 incubation, the membrane was moved to a new well with 100 µl of PEM and allowed to drain. The
368 membrane insert was then moved to a well containing 1200 µl of PEM block/permeabilization
369 solution (100 mM PIPES pH 6.9, 1 mM EGTA, 0.1 mM $MgSO_4$, 1% BSA, 0.3% Triton X-100) and
370 incubated for 30 minutes at room temperature. The membrane insert was moved to a well with
371 100 µl of PEM and allowed to drain and then moved into a well containing 1 mL PEM with DAPI

372 (2 µg/mL) and Phalloidin (0.1 µM) and incubated for 15 minutes at room temperature. Aggregates
373 were then washed once more in 1200 µl PEM. To mount aggregates for imaging, the membrane
374 insert was placed in a new well with 100 µl of PEM buffer and was allowed to drain, aggregates
375 were resuspended in the residual buffer (approximately 50 µl) by gentle pipetting, and then
376 aggregates were pipetted onto a microscope slide and allowed to settle for 5 minutes. Kimwipes
377 were then placed in contact with the edge of the liquid on the slide, allowing for removal of excess
378 buffer by capillary action. 15 µl of Fluoromount G (SouthernBiotech) was pipetted onto the
379 aggregates, which were then covered with a 22 x 40 mm cover glass and sealed with nail polish.
380 Aggregates were subsequently imaged with a Zeiss LSM 880 confocal microscope. Staining of
381 adherent cells with phalloidin was done as previously described (Parra-Acero et al., 2020).
382
383 EdU labeling of aggregates
384 To examine cell proliferation within aggregates by EdU labeling, aggregates were generated in
385 ultra-low adherence 24-well plates as described above. 3 days after aggregation was initiated,
386 100 µl of growth medium containing EdU was added to aggregates to result in a 150 µM EdU
387 concentration. Aggregates were incubated with EdU for 4 hours and then fixed and resuspended
388 in 300 µl PEM buffer as described above. Aggregates were then processed for imaging following
389 the manufacturer's protocol (ThermoFisher C10339) using the 24-well plate membrane insert
390 method described above to transfer aggregates between solutions. For all steps, wells with 1 mL
391 of solution were used for washing or staining cells in membrane inserts, and wells with 100 µl of
392 solution were used to drain wells in preparation for transfer into the next solution.
393
394 Molecular Biology
395 For the sequences of synthesized DNA fragments and oligonucleotides used in this study, see
396 Data S1 and S2, respectively. For a list of plasmids generated for this study, see Data S3. To
397 generate a vector for mScarlet expression in *Capsaspora* (pJP71), a DNA construct containing

398 an open reading frame encoding the mScarlet protein (Bindels et al., 2017) codon-optimized for
399 expression in *Capsaspora* and under control of the previously described EF1-α promoter and
400 terminator from the pONSY-mCherry vector (Parra-Acero et al., 2018) was constructed by gene
401 synthesis (sJP1) and cloned into the EcoRV site of the pUC57-mini vector (Genscript). A KpnI
402 site and an AflII site were incorporated at the beginning and end of the coding sequence,
403 respectively, allowing for the construction of N or C-terminal protein fusion constructs by Gibson
404 assembly. To generate a plasmid for expression of mScarlet and a Geneticin resistance gene
405 (pJP72), the NeoR coding sequence from the *Dictyostelium* pDM323 vector (Veltman et al., 2009)
406 was codon optimized for *Capsaspora*, the optimized sequence was synthesized with the promoter
407 and terminator from the *Capsaspora* actin ortholog gene CAOG_06018, and the synthesized
408 fragment (sJP2) was cloned into the SmaI site of pJP71 by Gibson assembly. To generate
409 plasmids expressing mScarlet and either nourseothricin resistance (pJP102) or hygromycin
410 resistance (pJP103), an identical strategy to that used in constructing pJP72 was used, except
411 either a synthesized codon-optimized nourseothricin acetyltransferase gene (sJP3) based on the
412 sequence of pUC18T-mini-Tn7T-nat (Lehman et al., 2016) or a synthesized codon-optimized
413 hygromycin B phosphotransferase gene (sJP4) based on the sequence of *Dictyostelium* vector
414 pDM358 (Veltman et al., 2009) was used.
415
416 To generate a plasmid encoding coYki and Hygromycin resistance for rescue of *coYki -/-*
417 phenotypes (pJP119), a DNA fragment encoding coYki and a c-terminal OLLAS epitope tag (Park
418 et al., 2008) was generated by PCR from a synthesized a gene encoding the coYki protein (sJP5)
419 using primers oJP101 and oJP102. To limit recombination of the transgene with the endogenous
420 coYki loci, we recoded the coYki reading frame using synonymous codon replacement, resulting
421 in a coYki gene with 73 percent nucleotide similarity to the WT coYki gene but encoding an
422 identical polypeptide. This PCR product was then cloned into a KpnI and AflII digest of pJP103
423 using Gibson assembly.

424

425 To generate a plasmid encoding a Lifeact-mScarlet fusion protein and hygromycin resistance
426 (pJP118), a DNA fragment optimized for expression in *Capsaspora* encoding the Lifeact peptide
427 (Riedl et al., 2008) (sJP6) was synthesized and cloned into the KpnI site of pJP103 by Gibson
428 assembly. To generate a plasmid expressing Venus and Geneticin resistance (pJP114), the
429 Venus reading frame was amplified from $p_{EF1\alpha}$ -CoH2B:Venus (Addgene #111877, (Parra-Acero
430 et al., 2018)) using primers oJP103 and oJP104 and cloned into a KpnI and AflII digest of pJP72
431 by Gibson assembly.

432

433 <u>*Capsaspora* Transfection</u>

434 24-well plates were prepared for transfection by inserting one sterile 12mm circular glass coverslip
435 in each well to aid in cell adhesion during transfection. *Capsaspora* cells at exponential growth
436 phase were collected by pipetting medium over attached cells, resuspended to 7.5 x 10^5 cells/ml
437 in growth medium, and then 800 µl of this cell culture was added per well to the prepared 24-well
438 plate. Cells were incubated at 23°C overnight. The following day growth medium was removed
439 from cells and was replaced by 800 µl of transfection medium (Scheider's Drosophila Medium
440 (ThermoFisher 21720024) with 10% FBS (ThermoFisher 26140079) supplemented with 25 µg/mL
441 Ampicillin). After a 10-minute incubation at room temperature, transfection medium was removed
442 from the cells and replaced with 500 of fresh transfection medium. Transfection mixes were then
443 prepared: 100 µl of Opti-MEM I Reduced Serum Medium (ThermoFisher) was added to a 1.5ml
444 tube, and 1 µg of transfecting DNA was added to this medium (for multiple plasmids, an equivalent
445 amount of each plasmid by mass was used). 3 µl of *Trans*IT-X2® transfection reagent (Mirus Bio)
446 was then added to the tube, and the solution was immediately mixed by pipetting up and down.
447 Transfection mixes were incubated at room temperature for 5 minutes, and then 70 µl of the
448 transfection mix was added dropwise to one well in the 24-well plate. Cells were incubated at
449 23°C for 24 hours, and then the medium was removed and replaced with 800 µl of growth medium.

450 To image fluorescent transient transfectants, cells were then resuspended by pipetting up and
451 down, and 300 µl of resuspended cells in growth medium were transferred to a well of an 8-well
452 chambered coverglass slide (Nunc). Cells were then imaged 48 hours after addition of growth
453 medium using a Zeiss LSM 880 confocal microscope.
454
455 Stable expression of transgenes in clonal *Capsaspora* cell lines
456 Transforming plasmids were linearized by digestion with either ScaI-HF® or AseI restriction
457 enzymes (NEB), which cut within the ampicillin resistance gene, and then purified from solution
458 and resuspended in nuclease-free water. *Capsaspora* cells were transfected with the linearized
459 plasmids using the *Trans*IT-X2® transfection reagent as described above. Two days after growth
460 medium was added to cells following transfection, the growth medium was removed and replaced
461 with 800 µl of growth medium supplemented with selective drugs. Due to observations of
462 variability in cell viability between transfections, three drug concentrations were tested in parallel
463 for each transfection: for Geneticin (ThermoFisher), cells were treated at 40, 60, or 80 µg/ml; for
464 Nourseothricin (GoldBio), cells were treated at 50, 75, or 100 µg/ml; for Hygromycin B (Sigma),
465 cells were treated at 150, 200, or 250 µg/ml. Cells were grown in selective medium for 2 weeks,
466 and medium was changed every 3 days. Following selection, clonal cell populations were
467 generated by resuspending cells in growth medium by pipetting, diluting cells to 3 cells/mL in
468 growth medium, and adding 100 µl of this dilution to 200 µl of growth medium per in a well in a
469 48-well plate (this procedure generated approximately 10 wells with cell growth for each 48-well
470 plate). To image fluorescence in stably transfected lines, clonal cell populations were transferred
471 into wells in a 4-well glass bottom chamber slide (Nunc), incubated at 23°C for 24 hours, and cells
472 were then imaged using a Nikon Eclipse Ti inverted microscope with NIS-Elements acquisition
473 software.
474
475 Disruption of the Capsaspora *coYki* gene by gene targeting

476 To disrupt *coYki,* we attempted to delete a 228 bp segment of the coYki open reading frame that
477 encodes the predicted Tead-binding domain (Sebe-Pedros et al., 2012) using a PCR-generated
478 gene targeting construct. We designed a pair of primers that amplify the drug resistance markers
479 described above, including the actin (CAOG_06018) promoter and terminator, with 90 bp of
480 homology adjacent to the sequence targeted for deletion at the 5' end of the primers (oJP105 and
481 oJP106). These primers were used to amplify the Geneticin resistance cassette from pJP72 by
482 PCR, the resulting PCR product was gel purified and resuspended in nuclease-free water, and
483 WT *Capsaspora* cells were transfected with this DNA as described above. Clonal populations of
484 drug-resistant transformants were generated as described above, each clone was grown to
485 confluency in one well in a 24-well plate, cells were collected by pipetting up and down, and
486 genomic DNA was prepared following the protocol described below. To genotype potential
487 mutants, we performed diagnostic PCRs on genomic DNA: to test for presence of the WT allele,
488 we used a forward primer with homology to the genome 5' of the *coYki* sequence targeted for
489 deletion (oJP107) and a reverse primer with homology within the sequence targeted for deletion
490 (oJP108). To detect successful deletion, we used oJP107 as a forward primer and a reverse
491 primer with homology to the geneticin resistance gene (oJP109). 40 percent of analyzed clones
492 (6 of 15 tested clones) showed a PCR product indicative of disruption of the *coYki* allele (Figure
493 S2D). However, all clones showed a band indicative of an intact WT *coYki* gene. We therefore
494 reasoned that, at least for the culture conditions used during transfection, *Capsaspora* cells may
495 be diploid.
496
497 After the isolation of clonal lines that were heterozygous for *coYki* disruption with the Geneticin
498 resistance marker as indicated by diagnostic PCR, we attempted to disrupt the remaining *coYki*
499 allele using nourseothricin resistance as a marker. pJP102 was used as a template for PCR using
500 primers oJP105 and oJP106 to generate a nourseothricin resistance cassette flanked by
501 homology arms targeting *coYki* for disruption. This construct was used to transfect a Geneticin-

502 resistant heterozygous coYki disruption mutant, and drug selection of transfectants was done as
503 described above using simultaneous selection with 60 µg/ml Geneticin and 75 µg/ml
504 nourseothricin. After generating clonal populations of drug-resistant transformants, diagnostic
505 PCR was done to detect the intact *coYki* allele as described above or a deletion allele containing
506 the nourseothricin resistance gene using primers oJP107 and oJP110. Two cell lines that showed
507 absence of the WT *coYki* allele and presence of both disruption alleles encoding either Geneticin
508 or nourseothricin resistance were used for subsequent phenotypic studies.
509
510 To quantify *coYki* gene expression in a putative homozygous *coYki* disruption mutant (*coYki-/-*)
511 by qPCR, 5 x 10^6 WT or *coYki-/-* cells were collected from culture flasks while in growth medium
512 by pipetting up and down, and RNA was isolated using a RNeasy Mini Plus kit (Qiagen). cDNA
513 was made using the iScript cDNA Synthesis Kit (BioRad), qPCR reactions were made using iQ™
514 SRBR® Green Supermix (BioRad), and qPCR was performed using a CFX96 Touch Real-time
515 PCR detection system (BioRad) with the following primers: oJP111 and oJP112 to detect GAPDH,
516 oJP113 and oJP114 to detect a region of coYki within the sequence targeted for deletion, and
517 oJP115 and oJP116 to detect a region coYki 3' of the sequence targeted for deletion.
518
519 Preparing *Capsaspora* genomic DNA
520 Capsaspora genomic DNA was prepared for PCR analysis following a procedure previously
521 developed for *Dictyostelium discoideum* (Charette and Cosson, 2004). Cells grown in a 24-well
522 or 48-well plate in growth medium were collected by pipetting up and down, pipetted into a 1.5
523 mL tube, centrifuged at 4000 x g for 5 minutes, and resuspended in 20 µl of nuclease-free water.
524 20 µl of Lysis buffer (50 mM KCl, 10 mM TRIS pH 8.3, 2.5 mM $MgCl_2$, 0.45% NP40, 0.45% Tween
525 20, and 800 µg/ml Proteinase K added fresh from a 20 mg/ml stock) was added to cells, which
526 were then incubated at room temperature for 5 minutes. Tubes were then placed at 95°C for 5

527 minutes. After cooling to room temperature, 1 µl of this sample was then used as a template in a
528 20-µl diagnostic PCR.
529
530 Quantification of aggregate size and circularity
531 ImageJ was used to quantify aggregate size and circularity using aggregate images. Images were
532 converted to 8-bit format, processed twice using the "Smooth" function, and a Threshold was
533 adjusted for each individual image. The Analyze Particles command was then run with a gate for
534 particle size at 400-infinity micron^2 and the "exclude on edges" option selected. The returned
535 values for aggregate area and circularity were then used for further analysis. Values
536 corresponding to more than one adjacent aggregate interpreted by the algorithm as a single
537 particle were discarded.
538
539 Assaying cell-cell adhesion and cell-substrate adhesion
540 To examine cell-cell adhesion, cells were collected from a culture flask by pipetting growth media
541 over the culture surface, diluted to 1 x 10^6 cells/mL in growth medium, and vortexed to disrupt cell
542 clusters. 1 mL volumes of cell culture were then transferred to 1.5 mL tubes and incubated on a
543 Labquake™ rotator (Thermo) for one hour at room temperature. Cultures were then examined by
544 hemocytometer, and the number of cells in each cluster of cells was counted for at least 35 cell
545 clusters for each independent experiment.
546
547 To examine cell-substrate adhesion, cells were diluted to 5 x 10^5 cells/mL in growth medium, and
548 3 mL volumes of culture were transferred per well to 6-well tissue culture-treated polystyrene
549 plates (Sigma CLS3506) and incubated at 23°C for 48 hours. For agitation, plates were then
550 placed on an orbital shaker and shaken at 140 RPM for 10 minutes, and then the medium from
551 each well ("disassociated fraction") was transferred to a separate tube and 3 mL of new growth
552 medium was added to each well. 3 µL of 500 mM EDTA was then added to each well to detach

553 cells from the culture surface, medium was pipetted up and down over the culture surface 20
554 times, and this resuspension ("adherent fraction") was transferred to a separate tube. Cell
555 densities of the collected fractions were determined by hemocytometer counts, total cell amounts
556 were calculated by adding the cell numbers for disassociated and adherent fractions for each
557 condition, and the percent of adherent cells for each condition was then calculated. As a control
558 to examine cell-substrate adhesion in the absence of agitation, the above protocol was followed,
559 except the orbital shaker agitation step was omitted.
560
561 Time-lapse Microscopy
562 To image cells by time-lapse transmitted light or fluorescence microscopy, cells were
563 resuspended to 1 x 10^8 cells/ml in growth medium, and 10 µl of this cell suspension was added
564 as a spot in the center of a well in a 4-well chambered coverglass slide (Nunc). After a 1 hour
565 incubation at room temperature to allow the cells to settle, the 10 µl volume of medium was
566 removed, and 1 ml of growth medium was added to the well, resulting in a spot of cells in the
567 center of the well. Cells were incubated at room temperature for 24 hours, a field of view with
568 well-spaced cells was located, and then cells were imaged by time-lapse microscopy using a
569 Nikon Eclipse Ti inverted microscope with NIS-Elements acquisition software. To image the effect
570 of blebbistatin on individual cells, similar imaging of cells was done, except that cells were treated
571 with either DMSO or 1 µm bebbistatin (Sigma B0560) for one hour before imaging. To image
572 aggregates by time-lapse microscopy, aggregates were generated in ultra-low attachment plates
573 as described above. During aggregate formation, 4-well chambered coverglass slides (Nunc)
574 were coated with UltraPure agarose (ThermoFisher) by making a 1% agarose in nuclease-free
575 water mixture, microwaving to dissolve the agarose, adding 800 µl of molten agarose per well,
576 and removing the molten agarose after 10 seconds by aspiration. Coated wells were then allowed
577 to dry at room temperature in a cell culture hood, resulting in a thin coating of agarose. This
578 coating functions to prevent aggregate adhesion to the glass surface. After aggregate formation,

579 aggregates were resuspended in the well by gentle pipetting, and then an 800 µl volume of
580 resuspended aggregates was transferred into one agarose-coated well in a 4-well chambered
581 coverglass slide. Aggregates were then imaged using a Zeiss LSM 880 confocal microscope.
582
583 RNA-seq
584 To perform RNA-seq on *Capsaspora* cells, WT or *coYki -/-* cells were collected from growth flasks
585 by removing growth medium, adding fresh growth medium, and resuspending cells attached to
586 the flask by pipetting the medium over the surface. Cells were then diluted to 2 x 10^5 cells/mL,
587 and for each genotype two 75 cm^2 culture flasks were prepared by adding 16 mL of culture dilution
588 to each flask. Culture flasks were incubated at 23°C for 2 days, and then cells were collected by
589 pipetting growth medium over attached cells. Cells were collected by centrifugation at 2100 x g
590 for 5 minutes, and then all cells for each genotype were combined, resuspended in 500 µl of
591 growth medium, and transferred to a microcentrifuge tube. RNA was then prepared with the
592 RNEasy Plus Mini Kit (Qiagen) using the QIAshredder spin column (Qiagen) to homogenize the
593 lysate. RNA samples were run on an Agilent Tapestation 4200 to determine level of degradation,
594 thus ensuring only high quality RNA was used (RIN Score 8 or higher). A Qubit® 4.0 Fluorimeter
595 (ThermoFisher) was used to determine the concentration prior to staring library prep. One
596 microgram of total DNAse-treated RNA was then prepared with the TruSeq Stranded mRNA
597 Library Prep Kit (Illumina). Poly-A RNA was purified and fragmented before strand specific cDNA
598 synthesis. cDNA was then A-tailed and indexed adapters were ligated. After adapter ligation,
599 samples were PCR-amplified and purified with AmpureXP beads, then validated again on the
600 Agilent Tapestation 4200. Before being normalized and pooled, samples were quantified by Qubit
601 then run on an Illumina NextSeq 500 using V2.5 reagents. Three biological replicates were
602 sequenced for each genotype, with 22-31 million reads generated per sample. The fastq files
603 were checked for quality using fastqc (v0.11.2)(Andrews, 2010) and fastq_screen
604 (v0.4.4)(Wingett, 2011). Fastq files were mapped to GCF_000151315.2 reference assembly

605 using STAR(Dobin et al., 2013). Read counts were then generated using featureCounts(Liao et
606 al., 2014). Trimmed Mean of M-values normalization and differential expression analysis were
607 performed using edgeR(Robinson et al., 2010) (false discovery rate (FDR) <=0.05, absolute
608 log2(fold change) >= 0.5, log(counts per million) >=0). Phylogenetic trees were downloaded from
609 PhyloDB(Huerta-Cepas et al., 2014) corresponding to *Capsaspora* (PhyID 101) and pairwise
610 distances for each gene were extracted using an R package ape (Paradis and Schliep, 2019).
611 Closest Human and mouse orthologues were then extracted and used to annotate the
612 *Capsaspora* genes. These annotated gene names were then used with IPA (Kramer et al., 2014)
613 (QIAGEN Inc., https://www.qiagenbioinformatics.com/products/ingenuity-pathway-analysis) to
614 get significantly enriched pathways in "Diseases and Bio Functions" category. To identify
615 functional enrichment in the sets of genes upregulated or downregulated in *coYki -/-* cells, DAVID
616 Functional Annotation Tool (Huang da et al., 2009) was used to identify functional categories with
617 FDR < 0.05 using all *Capsaspora* genome genes as the gene population background.
618
619 Statistics
620 All statistics were done using Prism (GraphPad software, San Diego, CA). Student's t-test was
621 done to compare differences between two groups, and one-way analysis of variance (ANOVA)
622 with a post-hoc test was used to compare differences among groups greater than two.
623
624 Gene nomenclature
625 In the manuscript we use italicized text to refer to a gene (e.g., *coYki)*, unitalicized text to refer
626 to a protein (e.g., coYki), "-/-" to indicate a homozygous deletion mutant (e.g., *coYki -/-),* and ">"
627 to indicate a promoter driving the expression of a gene (e.g., *EF1 > coYki).*

Acknowledgements:

We thank the McDermott Sequencing Core and the Next-Generation Sequencing Core for RNA sequencing, and Dr. Iñaki Ruiz-Trillo for sharing information on *Capsaspora* vectors. This work was supported in part by National Institute of Health grant EY015708 to D.P. During this work J.E.P was a Howard Hughes Medical Institute fellow of the Life Sciences Research Foundation. D.P. is an investigator of the Howard Hughes Medical Institute.

Author Contributions: JEP and DP conceived the study and designed experiments. JEP and MS performed experiments. JEP, MK, and CX analyzed RNAseq data. JEP, DP, and MK wrote the original manuscript draft. JEP, MS, DP, MK, and CX revised and edited the manuscript.

Competing interests: Authors declare that they have no competing interests.

Data and materials availability: RNAseq data generated in this study have been deposited into the NCBI SRA (Bioproject PRJNA759885). The following plasmids have been deposited at Addgene: pJP72 (#176479), pJP102 (#176480), pJP103 (#176481), and pJP118 (#176494).

646 **REFERENCES**

647 Andrews, S. (2010). FastQC: a quality control tool for high throughput sequence data. .
648 Available online at: http://wwwbioinformaticsbabrahamacuk/projects/fastqc.

649 Bindels, D.S., Haarbosch, L., van Weeren, L., Postma, M., Wiese, K.E., Mastop, M., Aumonier,
650 S., Gotthard, G., Royant, A., Hink, M.A.*, et al.* (2017). mScarlet: a bright monomeric red
651 fluorescent protein for cellular imaging. Nat Methods *14*, 53-56.

652 Blandin, A.F., Noulet, F., Renner, G., Mercier, M.C., Choulier, L., Vauchelles, R., Ronde, P.,
653 Carreiras, F., Etienne-Selloum, N., Vereb, G.*, et al.* (2016). Glioma cell dispersion is driven by
654 alpha5 integrin-mediated cell-matrix and cell-cell interactions. Cancer Lett *376*, 328-338.

655 Booth, D.S., and King, N. (2020). Genome editing enables reverse genetics of multicellular
656 development in the choanoflagellate Salpingoeca rosetta. Elife *9*.

657 Booth, D.S., Szmidt-Middleton, H., and King, N. (2018). Transfection of choanoflagellates
658 illuminates their cell biology and the ancestry of animal septins. Mol Biol Cell *29*, 3026-3038.

659 Charette, S.J., and Cosson, P. (2004). Preparation of genomic DNA from Dictyostelium
660 discoideum for PCR analysis. Biotechniques *36*, 574-575.

661 Charras, G., and Paluch, E. (2008). Blebs lead the way: how to migrate without lamellipodia.
662 Nat Rev Mol Cell Biol *9*, 730-736.

663 Charras, G.T., Hu, C.K., Coughlin, M., and Mitchison, T.J. (2006). Reassembly of contractile
664 actin cortex in cell blebs. J Cell Biol *175*, 477-490.

665 Coste, A., Jager, M., Chambon, J.P., and Manuel, M. (2016). Comparative study of Hippo
666 pathway genes in cellular conveyor belts of a ctenophore and a cnidarian. Evodevo *7*, 4.

667 Davis, J.R., and Tapon, N. (2019). Hippo signalling during development. Development *146*.

668 Deng, H., Yang, L., Wen, P., Lei, H., Blount, P., and Pan, D. (2020). Spectrin couples cell
669 shape, cortical tension, and Hippo signaling in retinal epithelial morphogenesis. J Cell Biol *219*.

670 Dobin, A., Davis, C.A., Schlesinger, F., Drenkow, J., Zaleski, C., Jha, S., Batut, P., Chaisson,
671 M., and Gingeras, T.R. (2013). STAR: ultrafast universal RNA-seq aligner. Bioinformatics *29*,
672 15-21.

673 Dumbauld, D.W., Shin, H., Gallant, N.D., Michael, K.E., Radhakrishna, H., and Garcia, A.J.
674 (2010). Contractility modulates cell adhesion strengthening through focal adhesion kinase and
675 assembly of vinculin-containing focal adhesions. J Cell Physiol *223*, 746-756.

676 Fairclough, S.R., Dayel, M.J., and King, N. (2010). Multicellular development in a
677 choanoflagellate. Curr Biol *20*, R875-876.

678 Fernandez, B.G., Gaspar, P., Bras-Pereira, C., Jezowska, B., Rebelo, S.R., and Janody, F.
679 (2011). Actin-Capping Protein and the Hippo pathway regulate F-actin and tissue growth in
680 Drosophila. Development *138*, 2337-2346.

681 Fisher, H.W., and Yeh, J. (1967). Contact inhibition in colony formation. Science *155*, 581-582.

682 Foty, R.A., and Steinberg, M.S. (2005). The differential adhesion hypothesis: a direct evaluation.
683 Dev Biol *278*, 255-263.

684 Gaspar, P., and Tapon, N. (2014). Sensing the local environment: actin architecture and Hippo
685 signalling. Current opinion in cell biology *31*, 74-83.

686 Harvey, K.F., and Hariharan, I.K. (2012). The hippo pathway. Cold Spring Harb Perspect Biol *4*,
687 a011288.

688 Huang da, W., Sherman, B.T., and Lempicki, R.A. (2009). Bioinformatics enrichment tools:
689 paths toward the comprehensive functional analysis of large gene lists. Nucleic Acids Res *37*, 1-
690 13.

691 Huerta-Cepas, J., Capella-Gutierrez, S., Pryszcz, L.P., Marcet-Houben, M., and Gabaldon, T.
692 (2014). PhylomeDB v4: zooming into the plurality of evolutionary histories of a genome. Nucleic
693 Acids Res *42*, D897-902.

694 Ikmi, A., Gaertner, B., Seidel, C., Srivastava, M., Zeitlinger, J., and Gibson, M.C. (2014).
695 Molecular evolution of the Yap/Yorkie proto-oncogene and elucidation of its core transcriptional
696 program. Mol Biol Evol *31*, 1375-1390.

697 King, N., Hittinger, C.T., and Carroll, S.B. (2003). Evolution of key cell signaling and adhesion
698 protein families predates animal origins. Science *301*, 361-363.

699 Kramer, A., Green, J., Pollard, J., Jr., and Tugendreich, S. (2014). Causal analysis approaches
700 in Ingenuity Pathway Analysis. Bioinformatics *30*, 523-530.

701 Lehman, S.S., Mladinich, K.M., Boonyakanog, A., Mima, T., Karkhoff-Schweizer, R.R., and
702 Schweizer, H.P. (2016). Versatile nourseothricin and streptomycin/spectinomycin resistance
703 gene cassettes and their use in chromosome integration vectors. J Microbiol Methods *129*, 8-
704 13.

705 Liao, Y., Smyth, G.K., and Shi, W. (2014). featureCounts: an efficient general purpose program
706 for assigning sequence reads to genomic features. Bioinformatics *30*, 923-930.

707 Moya, I.M., and Halder, G. (2018). Hippo-YAP/TAZ signalling in organ regeneration and
708 regenerative medicine. Nature reviews Molecular cell biology.

709 Nichols, S.A., Roberts, B.W., Richter, D.J., Fairclough, S.R., and King, N. (2012). Origin of
710 metazoan cadherin diversity and the antiquity of the classical cadherin/beta-catenin complex.
711 Proc Natl Acad Sci U S A *109*, 13046-13051.

712 Paczkowska, M., Barenboim, J., Sintupisut, N., Fox, N.S., Zhu, H., Abd-Rabbo, D., Mee, M.W.,
713 Boutros, P.C., Drivers, P., Functional Interpretation Working, G.*, et al.* (2020). Integrative
714 pathway enrichment analysis of multivariate omics data. Nat Commun *11*, 735.

715 Paradis, E., and Schliep, K. (2019). ape 5.0: an environment for modern phylogenetics and
716 evolutionary analyses in R. Bioinformatics *35*, 526-528.

717 Park, S.H., Cheong, C., Idoyaga, J., Kim, J.Y., Choi, J.H., Do, Y., Lee, H., Jo, J.H., Oh, Y.S., Im,
718 W.*, et al.* (2008). Generation and application of new rat monoclonal antibodies against synthetic
719 FLAG and OLLAS tags for improved immunodetection. J Immunol Methods *331*, 27-38.

720 Parra-Acero, H., Harcet, M., Sanchez-Pons, N., Casacuberta, E., Brown, N.H., Dudin, O., and
721 Ruiz-Trillo, I. (2020). Integrin-Mediated Adhesion in the Unicellular Holozoan Capsaspora
722 owczarzaki. Curr Biol *30*, 4270-4275 e4274.

723 Parra-Acero, H., Ros-Rocher, N., Perez-Posada, A., Kozyczkowska, A., Sanchez-Pons, N.,
724 Nakata, A., Suga, H., Najle, S.R., and Ruiz-Trillo, I. (2018). Transfection of Capsaspora
725 owczarzaki, a close unicellular relative of animals. Development *145*.

726 Pires-daSilva, A., and Sommer, R.J. (2003). The evolution of signalling pathways in animal
727 development. Nat Rev Genet *4*, 39-49.

728 Porazinski, S., Wang, H., Asaoka, Y., Behrndt, M., Miyamoto, T., Morita, H., Hata, S., Sasaki,
729 T., Krens, S.F.G., Osada, Y.*, et al.* (2015). YAP is essential for tissue tension to ensure
730 vertebrate 3D body shape. Nature *521*, 217-221.

731 Riedl, J., Crevenna, A.H., Kessenbrock, K., Yu, J.H., Neukirchen, D., Bista, M., Bradke, F.,
732 Jenne, D., Holak, T.A., Werb, Z.*, et al.* (2008). Lifeact: a versatile marker to visualize F-actin.
733 Nat Methods *5*, 605-607.

734 Robinson, M.D., McCarthy, D.J., and Smyth, G.K. (2010). edgeR: a Bioconductor package for
735 differential expression analysis of digital gene expression data. Bioinformatics *26*, 139-140.

736 Ros-Rocher, N., Perez-Posada, A., Leger, M.M., and Ruiz-Trillo, I. (2021). The origin of
737 animals: an ancestral reconstruction of the unicellular-to-multicellular transition. Open Biol *11*,
738 200359.

739 Saias, L., Gomes, A., Cazales, M., Ducommun, B., and Lobjois, V. (2015). Cell-Cell Adhesion
740 and Cytoskeleton Tension Oppose Each Other in Regulating Tumor Cell Aggregation. Cancer
741 Res *75*, 2426-2433.

742 Sebe-Pedros, A., Degnan, B.M., and Ruiz-Trillo, I. (2017). The origin of Metazoa: a unicellular
743 perspective. Nat Rev Genet *18*, 498-512.

744 Sebe-Pedros, A., Irimia, M., Del Campo, J., Parra-Acero, H., Russ, C., Nusbaum, C., Blencowe,
745 B.J., and Ruiz-Trillo, I. (2013). Regulated aggregative multicellularity in a close unicellular
746 relative of metazoa. Elife *2*, e01287.

747 Sebe-Pedros, A., Pena, M.I., Capella-Gutierrez, S., Anto, M., Gabaldon, T., Ruiz-Trillo, I., and
748 Sabido, E. (2016). High-Throughput Proteomics Reveals the Unicellular Roots of Animal
749 Phosphosignaling and Cell Differentiation. Dev Cell *39*, 186-197.

750 Sebe-Pedros, A., Roger, A.J., Lang, F.B., King, N., and Ruiz-Trillo, I. (2010). Ancient origin of
751 the integrin-mediated adhesion and signaling machinery. Proc Natl Acad Sci U S A *107*, 10142-
752 10147.

753 Sebe-Pedros, A., Zheng, Y., Ruiz-Trillo, I., and Pan, D. (2012). Premetazoan origin of the hippo
754 signaling pathway. Cell reports *1*, 13-20.

755 Stanley, S.M. (1973). An ecological theory for the sudden origin of multicellular life in the late
756 precambrian. Proceedings of the National Academy of Sciences of the United States of America
757 *70*, 1486-1489.

758 Stein, C., Bardet, A.F., Roma, G., Bergling, S., Clay, I., Ruchti, A., Agarinis, C., Schmelzle, T.,
759 Bouwmeester, T., Schubeler, D.*, et al.* (2015). YAP1 Exerts Its Transcriptional Control via
760 TEAD-Mediated Activation of Enhancers. PLoS Genet *11*, e1005465.

761 Stibbs, H.H., Owczarzak, A., Bayne, C.J., and DeWan, P. (1979). Schistosome sporocyst-killing
762 Amoebae isolated from Biomphalaria glabrata. J Invertebr Pathol *33*, 159-170.

763 Straight, A.F., Cheung, A., Limouze, J., Chen, I., Westwood, N.J., Sellers, J.R., and Mitchison,
764 T.J. (2003). Dissecting temporal and spatial control of cytokinesis with a myosin II Inhibitor.
765 Science *299*, 1743-1747.

766 Suga, H., Dacre, M., de Mendoza, A., Shalchian-Tabrizi, K., Manning, G., and Ruiz-Trillo, I.
767 (2012). Genomic survey of premetazoans shows deep conservation of cytoplasmic tyrosine
768 kinases and multiple radiations of receptor tyrosine kinases. Sci Signal *5*, ra35.

769 Suga, H., and Ruiz-Trillo, I. (2013). Development of ichthyosporeans sheds light on the origin of
770 metazoan multicellularity. Dev Biol *377*, 284-292.

771 Sun, S., and Irvine, K.D. (2016). Cellular Organization and Cytoskeletal Regulation of the Hippo
772 Signaling Network. Trends in cell biology *26*, 694-704.

773 Veltman, D.M., Akar, G., Bosgraaf, L., and Van Haastert, P.J. (2009). A new set of small,
774 extrachromosomal expression vectors for Dictyostelium discoideum. Plasmid *61*, 110-118.

775 Williams, L.M., and Gilmore, T.D. (2020). Looking Down on NF-kappaB. Mol Cell Biol *40*.

776 Wingett, S. (2011). FastQ Screen: quality control tool to screen a library of sequences in FastQ
777 format against a set of sequence databases. . Available online at:
778 http://wwwbioinformaticsbabrahamacuk/projects/fastq_screen.

779 Yu, F.X., Zhao, B., and Guan, K.L. (2015). Hippo Pathway in Organ Size Control, Tissue
780 Homeostasis, and Cancer. Cell *163*, 811-828.

781 Zanconato, F., Forcato, M., Battilana, G., Azzolin, L., Quaranta, E., Bodega, B., Rosato, A.,
782 Bicciato, S., Cordenonsi, M., and Piccolo, S. (2015). Genome-wide association between
783 YAP/TAZ/TEAD and AP-1 at enhancers drives oncogenic growth. Nat Cell Biol *17*, 1218-1227.

784 Zheng, Y., and Pan, D. (2019). The Hippo Signaling Pathway in Development and Disease. Dev
785 Cell *50*, 264-282.
786

787

788

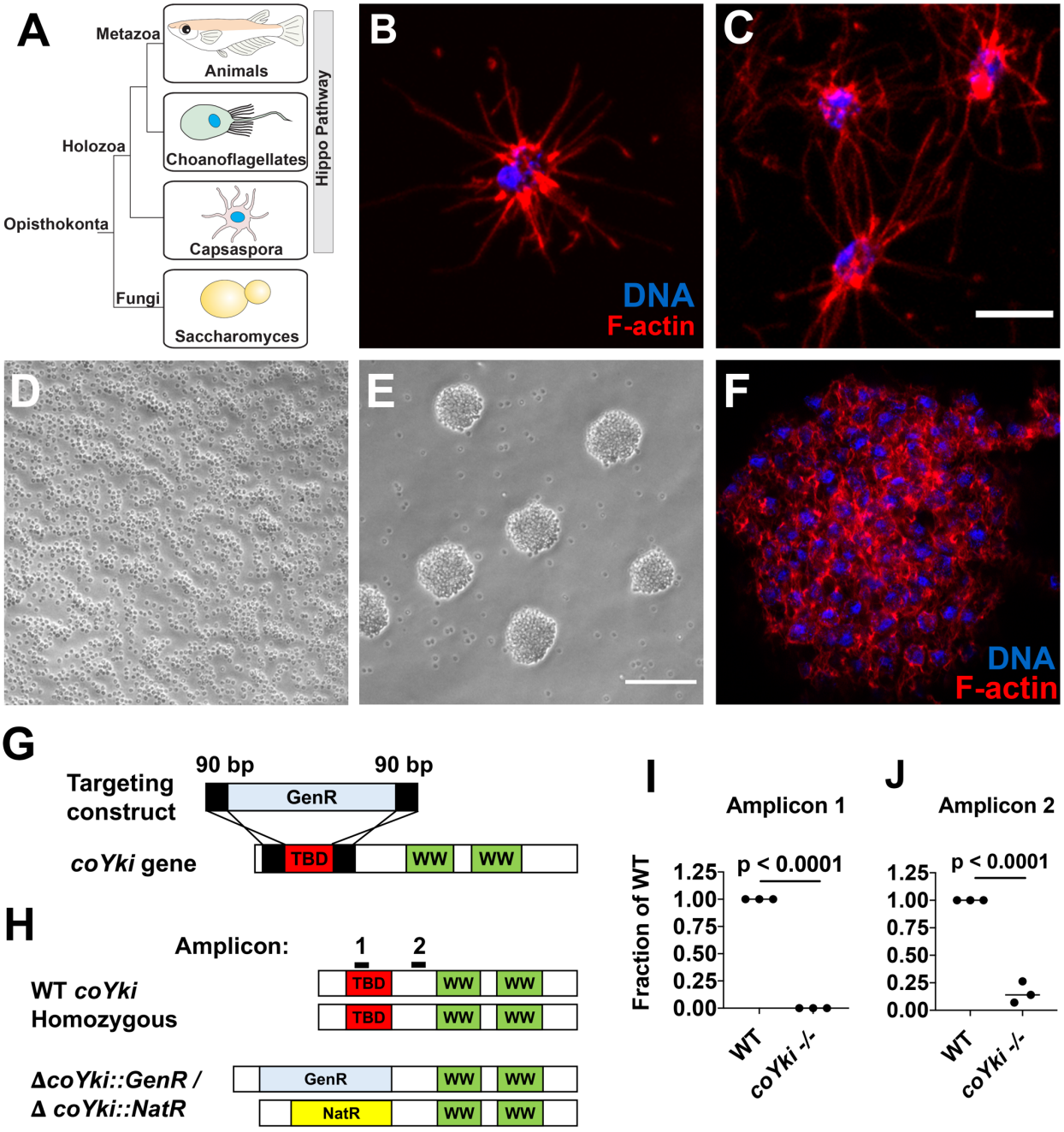

789

790

791 **Figure 1. Disruption of a YAP/TAZ/Yorkie ortholog in *Capsaspora*. (A)** Phylogenetic tree

792 showing conservation of the Hippo pathway in close unicellular relatives of animals. **(B)** A solitary

793 *Capsaspora* cell showing thin F-actin-enriched projections. Phalloidin and DAPI are used to stain

794 F-actin and DNA, respectively. **(C)** Cells at higher densities can contact other cells through
795 projections. Scale bar is 5 microns. **(D-E)** *Capsaspora* cells were inoculated into either a tissue-
796 culture treated plate **(D)** or a low-adherence plate **(E).** At 3 days, cells in standard plates grow as
797 a monolayer whereas cells in low-adherence plates form round aggregates. **(F)** An aggregate
798 stained for F-actin shows actin-rich connections between cells within an aggregate. Scale bar is
799 10 microns. **(G)** Strategy for disrupting the *coYki* gene by homologous recombination. GenR,
800 geneticin resistance cassette; TBD, Tead-binding domain; WW, WW domain. **(H)** Strategy for
801 demonstrating disruption of *coYki* by qPCR. Amplicon 1 corresponds to a region of the *coYki* gene
802 that should be absent in a homozygous mutant, whereas Amplicon 2 corresponds to a segment
803 of the gene 3' of the region targeted for deletion. **(I-J)** qPCR of Amplicons 1 and 2 in WT and
804 putative *coYki -/-* cells. The differences between WT and *coYki -/-* for both Amplicons 1 and 2 are
805 significant (t-test).
806 **See also Figure S1 and S2.**
807
808
809

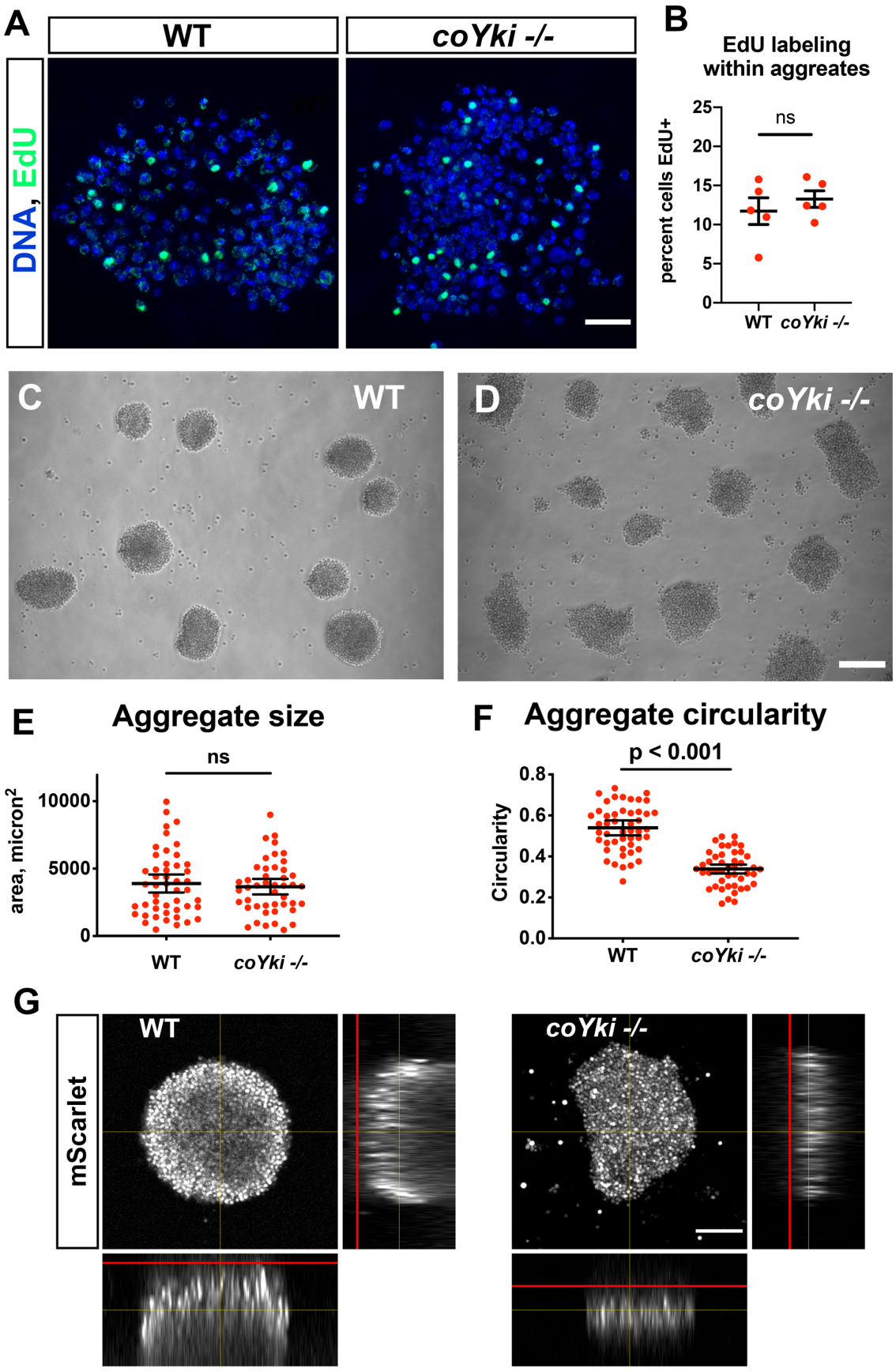
A
WT
coYki -/-
DNA, EdU
B
EdU labeling within aggreates
percent cells EdU+
ns
25
20
15
10
5
0
WT
coYki -/-
C
WT
D
coYki -/-
E
Aggregate size
ns
area, micron2
10000
5000
0
WT
coYki -/-
F
Aggregate circularity
p < 0.001
Circularity
0.8
0.6
0.4
0.2
0.0
WT
coYki -/-
G
mScarlet
WT
coYki -/-

811

812 **Figure 2. Loss of coYki results in no apparent effect on cell proliferation but alters the**
813 **morphology of multicellular aggregates. (A)** To examine proliferation within aggregates, EdU
814 was used to label proliferating cells within aggregates grown in low-adherence plates. **(B)** The
815 percent of cells positive for EdU within aggregates was quantified. Each red circle indicates
816 measurement results for a single aggregate, and mean ± SEM is shown in black. The difference
817 between WT ant *coYki -/-* cells is not significant (t-test). **(C-D)** WT or *coYki -/-* cells were inoculated
818 into low-adherence plates, and cell aggregates were imaged at 5 days. Scale bar is 75 microns.
819 **(E-F)** Aggregate size and circularity was measured from aggregate images using ImageJ. The
820 difference in aggregate circularity between WT and *coYki -/-* is significant (t-test). Bars indicate
821 the mean ± SEM (n=3 with 15 aggregates measured for each independent experiment), and dots
822 indicate values for individual aggregates. **(G)** Orthogonal views of WT and *coYki -/-* aggregates
823 are shown. Cell aggregates stably expressing mScarlet were imaged live by confocal microscopy.
824 Red lines show the location of the culture surface. Scale bar is 50 microns.
825 **See also Figure S3.**
826
827

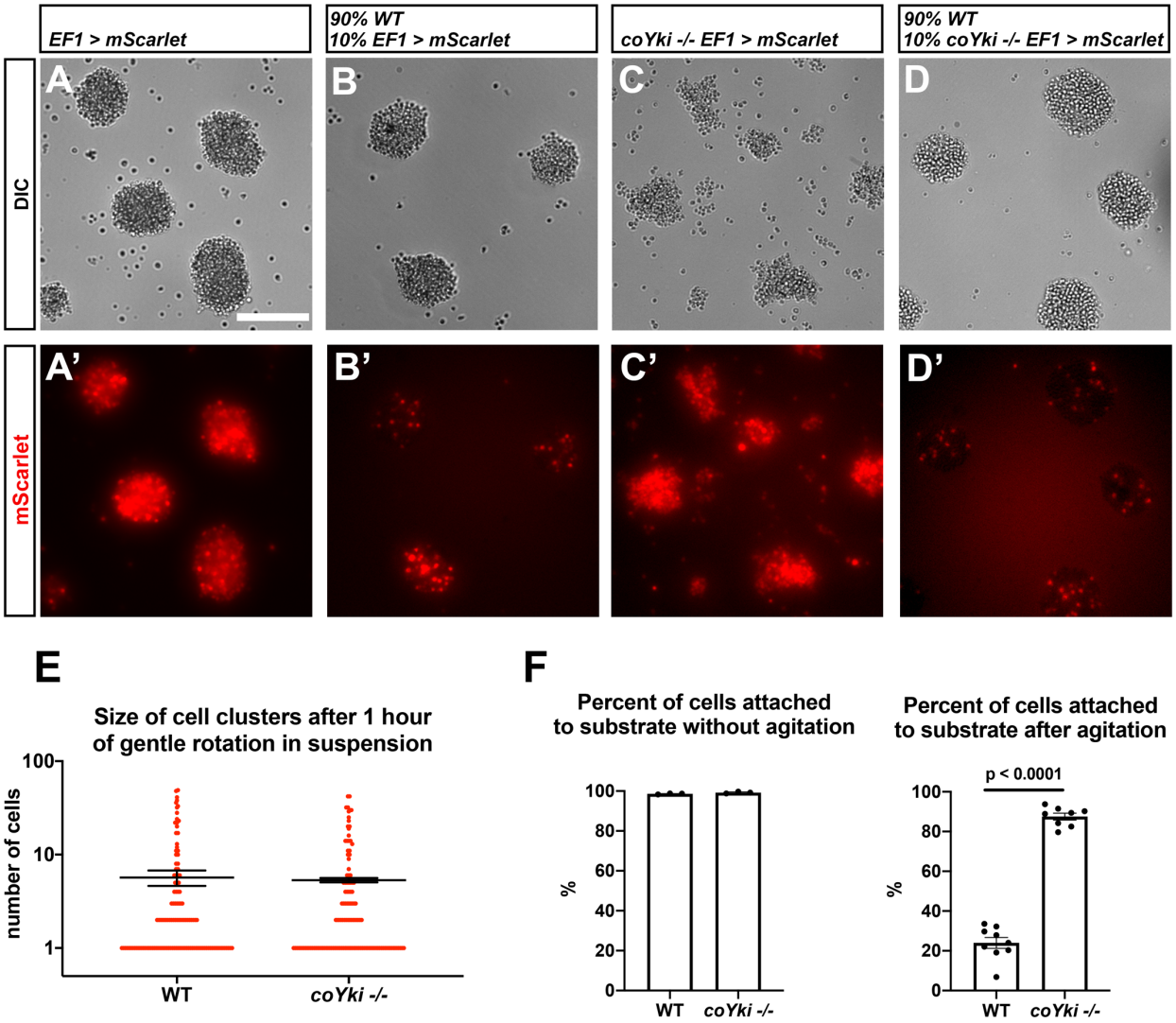

Figure 3. Loss of coYki affects cell-substrate adhesion but not cell-cell adhesion. (A-D) Cells expressing mScarlet in the WT background **(A-B)** or in the *coYki -/-* mutant background **(C-D)** were allowed to aggregate as a homogeneous population **(A, C)** or were mixed with 90% WT cells and allowed to aggregate **(B, D)**. Individual mScarlet-labeled *coYki -/-* cells associate with WT cells within aggregates **(D')** in an organization like that of cells from the WT background labeled with mScarlet **(B')**. Scale bar is 75 microns. **(E)** To examine cell-cell adhesion, cells in suspension were gently rotated for an hour to stimulate cluster formation through cell-cell adhesion. Cultures were then examined by hemocytometer and the number of cells per cluster was counted. Each red circle indicates the number of cells in a single cluster, and error bars

839 indicate the mean ± SEM of the average number of cells per cluster from 3 independent
840 experiments. Absence of error bars indicates that error is smaller than the plot symbol. The
841 difference in average number of cells per cluster between WT and *coYki -/-* is not significant (t-
842 test). **(F)** To examine cell-substrate adhesion, adherent cell cultures were either agitated on a
843 rotary shaker for 10 minutes or left untreated, and then the number of adhered and unadhered
844 cells in each culture was counted and the percent of cells adhered to the culture substrate was
845 calculated.
846

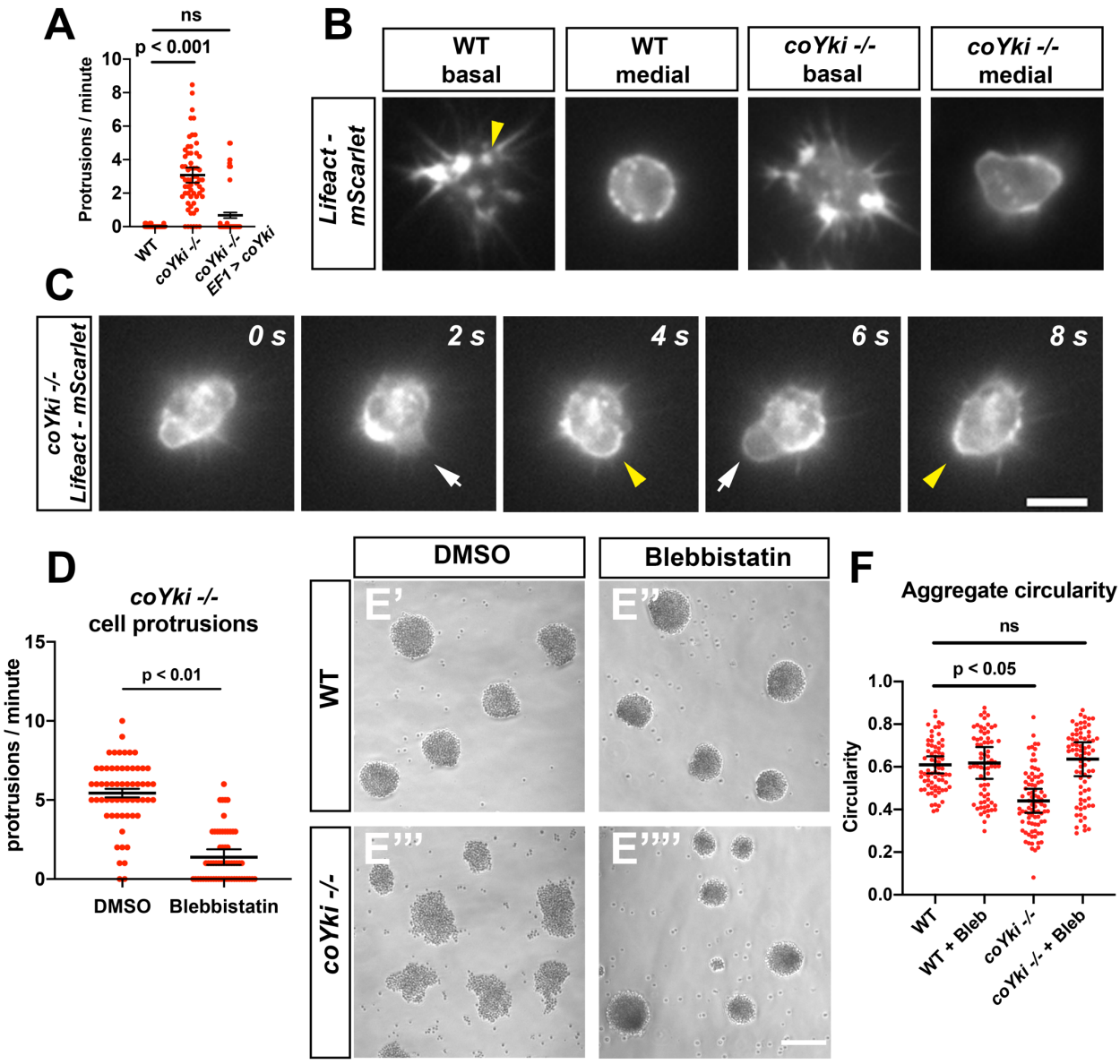

847

848

849 **Figure 4. Loss of coYki causes bleb-like protrusions at the cell cortex. (A)** *Capsaspora* cells
850 on a glass surface were imaged by time-lapse microscopy and individual cells were scored for
851 number of protrusions per minute. A protrusion is defined as a localized extension of the cell
852 boundary that disrupts a previously inert region of the cortex and/or changes the direction of
853 movement of the cell. Differences between WT and *coYki -/-* are significant (one-way ANOVA,
854 Tukey's test). Values from 3 independent experiments with 20 cells measured for each condition
855 per experiment are shown. Red dots indicate the measurement from an individual cell, and black

856 bars indicate the mean ± SEM of the means from each independent experiment. **(B)** Cells on a
857 glass surface stably expressing Lifeact-mScarlet were imaged focusing on the base of the cell at
858 the substrate ("basal") or at the mid-height of the cell ("medial"). Arrowhead shows an example of
859 Lifeact signal at the base of the cell that remains stationary as the cell moves (see Video S4).
860 Scale bar is 5 microns. **(C)** Time series of a *coYki -/-* cell stably expressing Lifeact-mScarlet on a
861 glass surface. White arrows indicate Lifeact-depleted bleb-like protrusions, and yellow
862 arrowheads indicate areas of cell cortex constriction, which correlate with increased Lifeact signal.
863 Scale bar is 5 microns. **(D)** Cells on a glass surface were treated with DMSO or 1 μM blebbistatin
864 for 1 hour, and then cells were imaged by time lapse microscopy and the number of protrusions
865 per cell was quantified. **(E)** Cells were inoculated into low-adherence plates with DMSO **(E',E''')**
866 or 1 μM blebbistatin **(E'',E'''')**, and aggregates were imaged after 5 days. Scale bar is 75 microns.
867 **(F)** Circularity of aggregates was measured with ImageJ using images of aggregates from the
868 indicated conditions. Black bars indicate the mean ± SEM (n=4 with 15 aggregates measured for
869 each independent experiment), and red dots indicate the measurements for individual
870 aggregates. Differences in circularity between WT and *coYki -/-* aggregates treated with DMSO
871 are significant (one-way ANOVA, Dunnett's test), whereas differences between WT aggregates
872 treated with DMSO and *coYki -/-* aggregates treated with blebbistatin are not. "Bleb" indicates
873 blebbistatin.

874
875

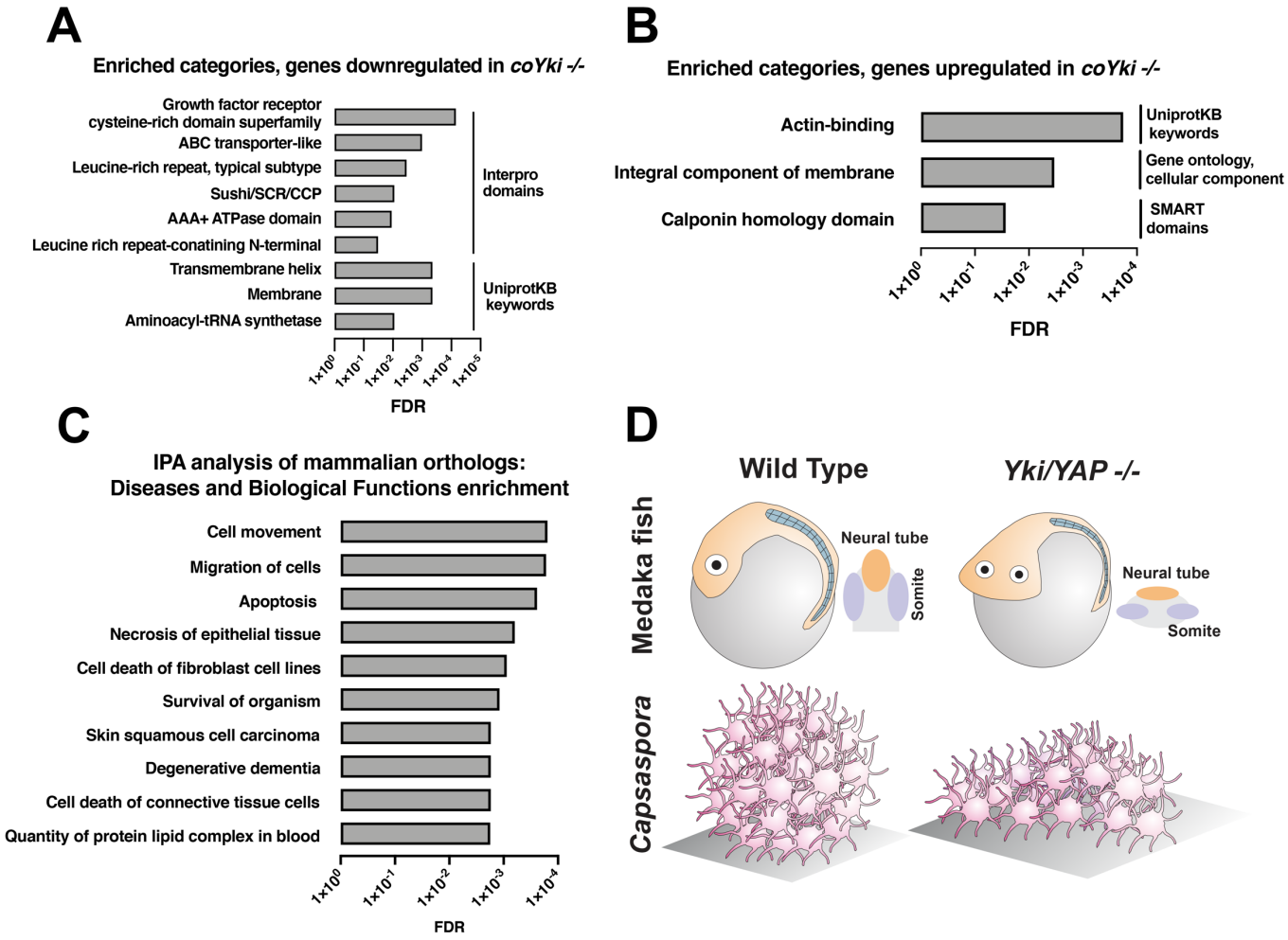

Figure 5. Functional enrichment of genes differentially expressed in *coYki -/-* cells. Top enriched categories from the sets of genes significantly downregulated **(A)** or upregulated **(B)** in *coYki -/-* cells compared to WT are shown. **(C)** Ingeneuity Pathway Analysis was performed on a set of predicted human/mouse orthologs of *Capsaspora* genes with significant changes in expression in *coYki -/-* cells. Enriched diseases and biological functions with false discovery rate (FDR) ≤ 0.05 are shown. **(D)** A schematic showing the flattened body phenotype of *YAP -/-* medaka fish embryos (top) and the flattened 3D shape of *coYki -/- Capsaspora* aggregates (bottom).

887 **SUPPLEMENTAL INFORMATION**
888

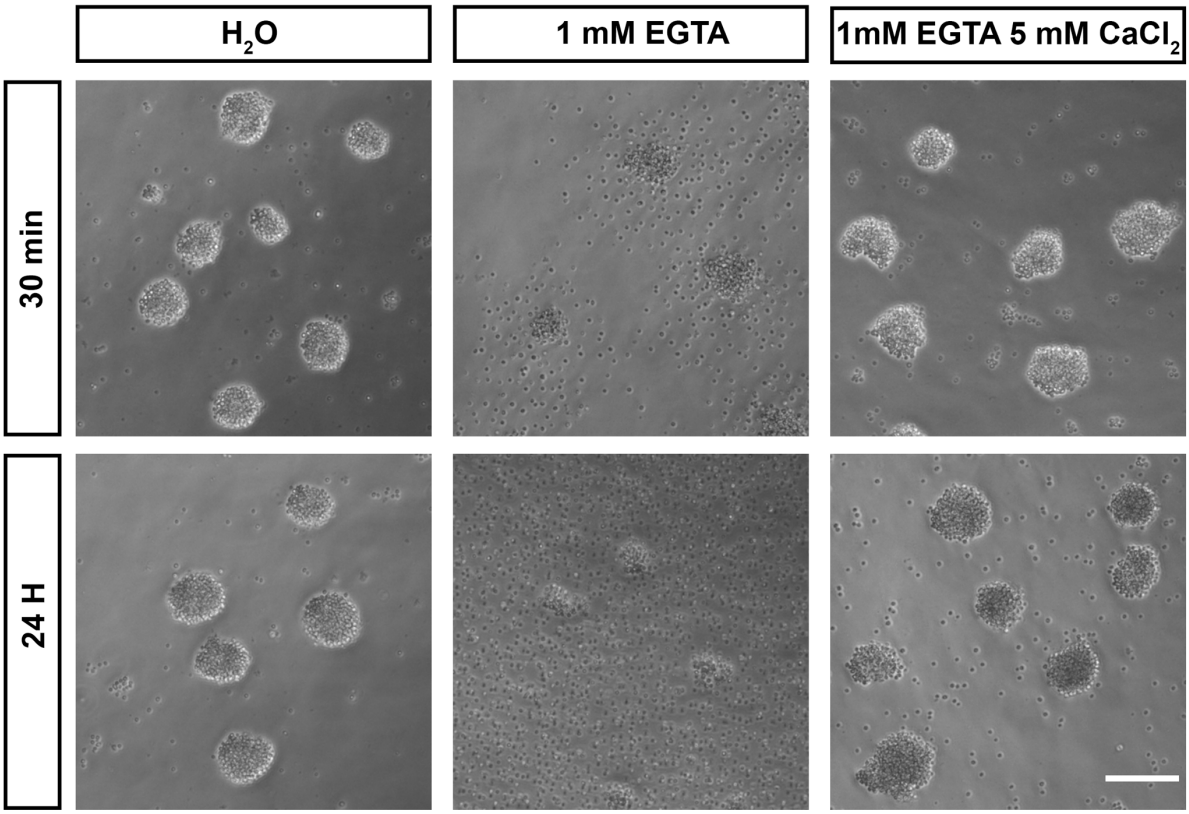

889

890 **Figure S1. Calcium is required for adhesion in *Capsaspora* cell aggregates, related to**
891 **Figure 1.** *Capsaspora* aggregates were treated with water (vehicle control), the calcium chelator
892 EGTA, or EGTA with an excess of calcium. At 30 minutes aggregates treated with EGTA had
893 begun to disassociate, with further disassociation evident at 24 hours. Simultaneous addition of
894 an excess of calcium blocked this disassociation.

895

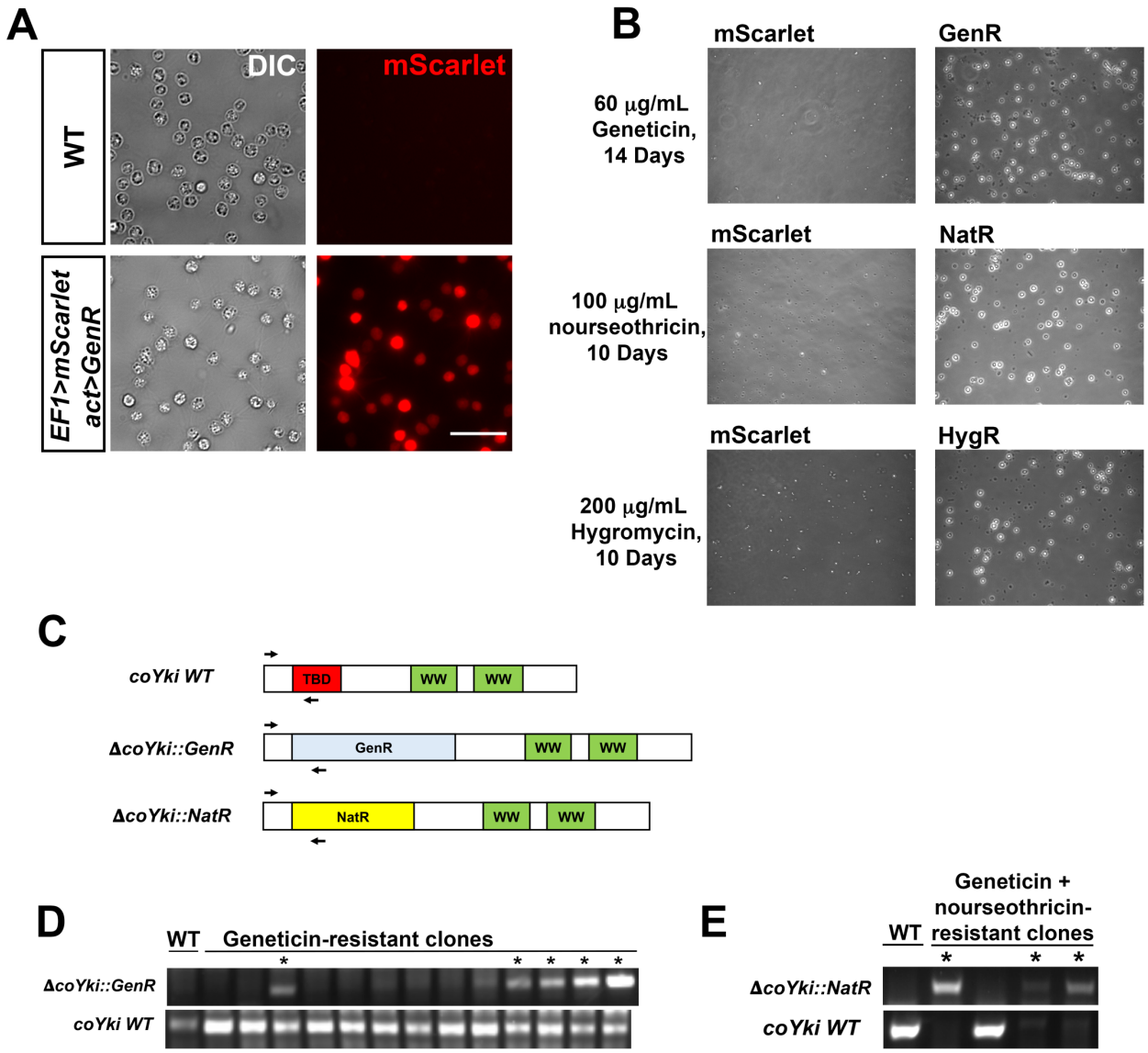

Figure S2. Stable transgene expression and confirmation of gene knockout in *Capsaspora*, related to Figure 1.

(A) WT *Capsaspora* cells and a clonal population of cells stably expressing mScarlet were imaged to show fluorescence. Scale bar is 20 microns. **(B)** Transfection of *Capsaspora* with genes encoding antibiotic resistance markers results in viable cell populations after drug treatment. Cells were transfected with plasmids encoding mScarlet with no antibiotic marker (pJP71), GenR

907 (pJP72), NatR (pJP102), or HygR (pJP103) genes and were treated with the indicated antibiotics
908 2 days after transfection for the indicated time period. Representative images of the population
909 are shown. Round, phase-bright cells are visible in populations transfected with resistance
910 markers but not cells transfected with mScarlet. **(C-E)** Diagnostic PCR of putative coYki deletion
911 clonal cell lines. **(C)** Diagram of primer pairs used to evaluate the presence of the WT *coYki* allele
912 (*coYki* WT), a deletion of a region of *coYki* using the GenR marker (Δ*coYki::GenR*), or a deletion
913 of a region of coYki using the NatR marker (Δ*coYki::NatR*). TBD, Tead-binding domain; WW, WW
914 domain; GenR, Geneticin resistance; NatR, nourseothricin resistance. **(D)** WT cells were
915 transfected with a gene-targeting construct encoding GenR designed to delete the TBD in the
916 *coYki* gene by homologous recombination (see figure 1G in main text). Following transfection and
917 drug selection, clonal populations of transfectants were generated and analyzed by diagnostic
918 PCR using the indicated primer pairs. "*" indicates a clone showing a PCR product indicative of
919 heterozygous coYki disruption. **(E)** A clonal cell line with a diagnostic PCR result indicating the
920 disruption of a coYki allele with GenR was transfected with a gene-targeting construct encoding
921 NatR designed to delete the TBD in the *coYki* gene. After selection with both Geneticin and
922 nourseothricin, clonal populations of transfectants were generated and analyzed by diagnostic
923 PCR using the indicated primer pairs. "*" indicates a clone showing a PCR product indicative of
924 homozygous coYki disruption.
925
926

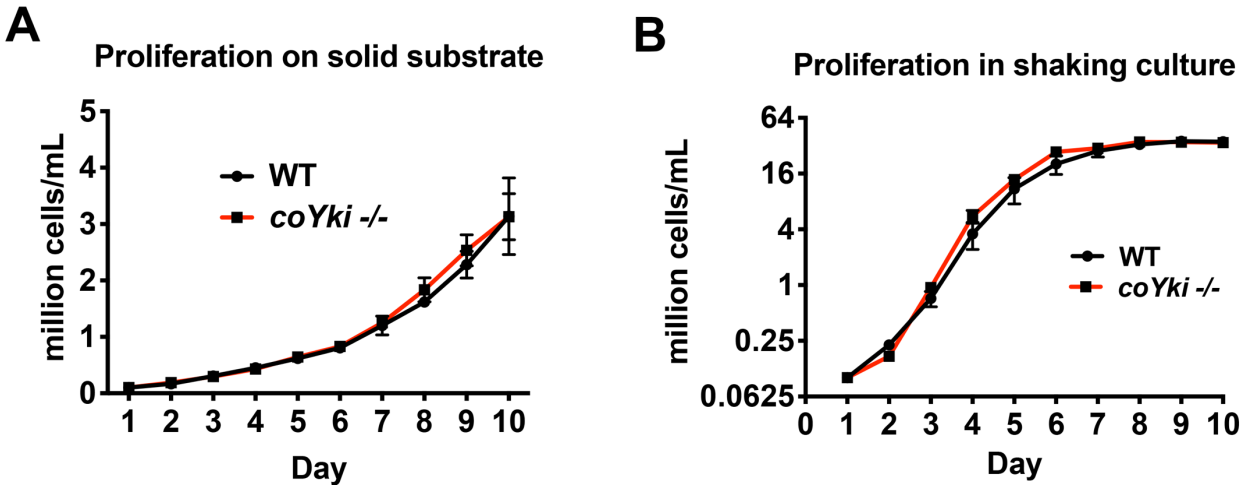

Figure S3. WT and *coYki -/-* cells proliferate at a similar rate, related to Figure 2.

(A) To examine proliferation on a solid substrate, cells were grown in wells in a 24-well plate, and each day cells within one well were resuspended and counted. **(B)** To examine proliferation in shaking culture, cells were grown in flasks on an orbital shaker, and an aliquot of cells was collected and counted daily. Values are mean ± SEM ($n \geq 3$). Absence of error bars indicates that error is smaller than the plot symbol.

937 **Video S1. Aggregation of WT or *coYki -/-* cells over 6 days on a low-adherence surface.**

938 Time units are given in days.

939

940 **Video S2. WT and *coYki -/-* cells on a glass surface.**

941

942 **Video S3. *coYki -/-* cells expressing a *coYki* rescue transgene.**

943

944 **Video S4. Basal region of *Capsaspora* cells expressing Lifeact-mScarlet.**

945

946 **Video S5. Medial region of WT or *coYki -/-* cells expressing Lifeact-mScarlet.**

947

948 **Video S6. Actin dynamics in a single *coYki -/-* cell expressing Lifeact-mScarlet.**

949

950 **Video S7. WT or *coYki -/-* cells expressing Lifeact-mScarlet within an aggregate.**

951

952 **Video S8. Treatment of *coYki -/-* cells expressing Lifeact-mScarlet with blebbistatin**

953 **reduces blebbing.**

954

955

956 **Data S1. Sequences of synthesized gene fragments used in this study**

957

958 **Data S2. Sequences of oligonucleotides used in this study**

959

960 **Data S3. Plasmids constructed for this study**

961